

ESTIMATING SEAL PUP PRODUCTION IN THE GREENLAND SEA USING BAYESIAN HIERARCHICAL MODELING

MARTIN JULLUM¹, THORDIS THORARINSDOTTIR², AND FABIAN E. BACHL³

ABSTRACT. The Greenland Sea is an important breeding ground for harp and hooded seals. Estimates of the annual seal pup production are critical factors in the abundance estimation needed for management of the species. These estimates are usually based on counts from aerial photographic surveys. However, only a minor part of the whelping region can be photographed, due to its large extent. To estimate the total seal pup production, we propose a Bayesian hierarchical modeling approach motivated by viewing the seal pup appearances as a realization of a log-Gaussian Cox process using covariate information from satellite imagery as a proxy for ice thickness. For inference, we utilize the spatial partial differential equation (SPDE) module of the integrated nested Laplace approximation (INLA) framework. In a case study using survey data from 2012, we compare our results with existing methodology in a comprehensive cross-validation study. The results of the cross validation study indicate that our method improves local estimation performance, and that the increased prediction uncertainty of our method is required to obtain calibrated count predictions. This suggests that the sampling density of the survey design may not be sufficient to obtain reliable estimates of the seal pup production.

1. INTRODUCTION

Three stocks of harp seals (*Pagophilus groenlandicus*) and two (possibly three) stocks of hooded seals (*Cystophora cristata*) inhabit the North Atlantic Ocean where they have been harvested for centuries (Sergeant, 1974, 1991; Kovacs & Lavigne, 1986). Monitoring the abundance of seals is vital for controlling the biodiversity in the region. State-of-the-art seal population models are dynamically built based on historical catch data (Øigård et al., 2014a,b). The main ingredient in these models is the total pup production in a given year which needs to be quantified based on on-site observational data since other quantification methods based on catch-at-age and mark-recapture data etc. are considered unreliable (ICES, 2014). The whelping regions in the North Atlantic typically cover several thousand square kilometers so that the total pup production needs to be estimated based on observations from a minor part of the region. The estimated total pup production and the associated uncertainty then enter the dynamic population model (Øigård et al., 2010).

The observational data consists of seal pup counts obtained by manual counting on photographs stemming from an aerial photographic survey conducted by flying along transects sparsely covering the whelping region. The survey methodology is discussed in more detail in Section 2. The traditional method for estimating the total pup production based on such count data is that of Kingsley et al. (1985) which assumes a homogeneous dispersion of seals across the entire whelping region. Salberg et al. (2009) propose a generalized additive modeling (GAM) approach (Hastie & Tibshirani, 1990), assuming the counts follow a negative binomial distribution and taking the spatial location of the counts into account. For data that is close to homogeneous, the negative binomial GAM approach and the Kingsley method yield similar estimates. However, the Kingsley method may possess a positive bias when the spatial distribution of the pups is clustered (Salberg et al., 2008; Øigård et al., 2010). Additionally, the GAM method produces much smaller uncertainty bounds than the homogeneous Kingsley approach.

^{1,2}NORWEGIAN COMPUTING CENTER, OSLO, NORWAY.

³SCHOOL OF MATHEMATICS, UNIVERSITY OF EDINBURGH, EDINBURGH, SCOTLAND.

E-mail addresses: jullum@nr.no, thordis@nr.no, bachlfab@gmail.com.

In this paper, we propose a new method for estimating the total seal pup production. We view the seal pup appearances as a spatial point process (Møller & Waagepetersen, 2003) and model the point pattern of the seal pups as a log-Gaussian Cox process (LGCP; Møller et al., 1998) with a spatial latent field which also allows additional covariate information to be accounted for. In a Bayesian formulation with priors on the model parameters, the seal pup abundance estimate is represented by the posterior predictive distribution found by integrating the posterior distribution over the spatial domain of the whelping region, instead of a single point estimate accompanied with a variance estimate. This Bayesian hierarchical model can be fitted by utilizing the spatial partial differential equation (SPDE) approach of the integrated nested Laplace approximation method (INLA; Lindgren et al., 2011; Rue et al., 2009). The final posterior predictive distribution can subsequently be computed from this fitted model by a sampling approach. Although more traditional Markov Chain Monte Carlo (MCMC) methods in theory could be used to arrive at the same posterior, application of INLA allows results to be produced magnitudes faster, in a convenient fashion, at a negligible cost in terms of accuracy.

To illustrate and test this methodology, we use seal pup photo counts from an aerial photographic survey in the Greenland Sea in March 2012 with two different types of seals, harp and hooded seals. The data set contains the spatial location of each photo and the corresponding pup count. To be more informative about the non-observed areas, we include covariate information extracted from satellite imagery captured on the very same date as the aerial photographic survey was conducted, to act as a proxy for ice thickness. Compared to the two other procedures our method gives larger uncertainties, especially for the harp seals. To validate these differences, we compare our proposed method with a number of reference methods in a comprehensive validation scheme. The scheme suggests our method performs best on local level, and comparable on a more global scale. Further investigations suggest that the larger uncertainty in our method is indeed more realistic.

The rest of the paper is organized as follows: Section 2 describes the surveying method used to gather seal pup observational data, in addition to specific details related to our particular seal pup data set. The satellite imagery and the covariate information extracted therefrom are also discussed. Section 3 is the main section of the paper. It starts by giving some background to our modeling approach through brief introductions to the relevant parts of point processes and the INLA framework, before going into detail about the present modeling approach. Subsequently, we discuss the reference approaches in more detail, before we describe the validation scheme used to verify and compare the different approaches. The results are presented in Section 4, including both specifics of the model fitted with our procedure, and the model comparison results. The final Section 5 contains concluding remarks and pointers to further work.

2. DATA

In this section we describe the surveying method and additional modeling information we have obtained through satellite imagery.

2.1. Survey method. Before conducting the aerial photographic survey with the purpose of monitoring the seal pup production, the marine researchers typically perform a helicopter reconnaissance survey. This is done in order to locate the patches where the seals whelp for limiting the survey area for the more expensive airborne photographic survey. The actual photographic survey is conducted by flying a survey aircraft equipped with advanced photographic equipment and GPS along a number of transects at a fixed distance that sparsely cover the survey area.

In this particular survey in March 2012, the airplane flew at an altitude of about 330m, and took a total of 2792 photos along 27 parallel transects, approximately 3Nm (≈ 5.6 km) apart, with each photo covering 226×346 m of ground level. Due to fog, an exception was made for the two southernmost transects, which were flown at an altitude of 250m, with the photos covering 170×260 m. Along each transect, the cameras were turned on when the first seal was spotted from the airplane, and photos were taken continuously until the ice edge was reached on the eastern side, and until no seals were spotted for an extended period to the west. As a

consequence of this survey setup, the whelping region is approximately defined as the union of the $1.5Nm$ ($\approx 2.8\text{km}$) bands around each transect. Thus, when estimating the total pup production in the whelping region, we only count predictions within this area. More details about the survey may be found in [Øigård et al. \(2014a,b\)](#).

2.2. Seal pup counts. Following the airborne survey, experienced marine researchers manually count the number of seal pups of each species in each photo. Quality checks with multiple examinations are performed to limit the measurement error introduced in this step ([Øigård et al., 2014a,b](#)). The seal pup count data set used on the subsequent analysis contains the coordinates and extent of each photo, in addition to the number of seal pups of each species observed. The data are plotted in [Figure 1](#) along with the transect locations and the extent of the whelping region. As seen from the figure, there tends to be more seal types clustered towards the middle eastern boundary and southern corner of the whelping region. Comparatively more harp seal pups are observed than hooded seal pups and the spatial distribution of the former seems less homogeneous.

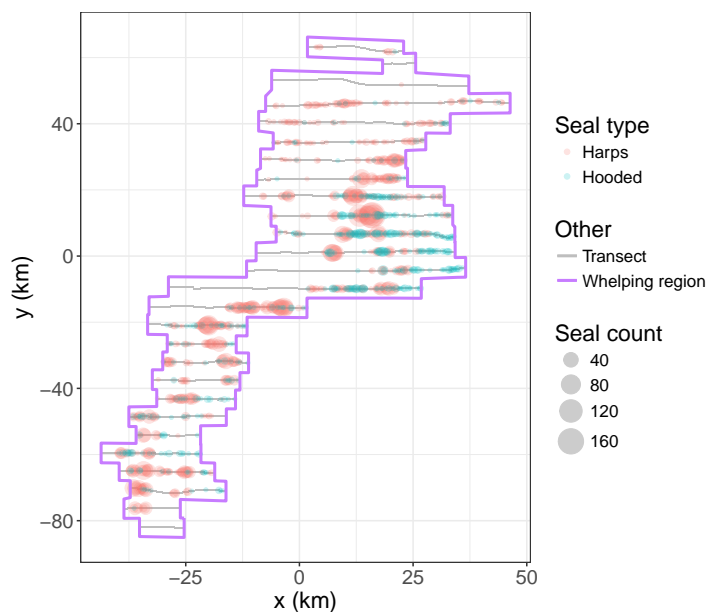


FIGURE 1. Harp and hooded seal pup count data from the Greenland Sea 2012 survey, with east-west direction on the x -axis and north-south direction on the y -axis.

2.3. Satellite imagery. For whelping, the seals require large ice floes with access to the ocean for the adult seals to access food. Information regarding which areas are covered by ice floes and which areas are merely open water, is thus potentially highly relevant when estimating the seal pup production. In an attempt to account for this, we have collected high resolution satellite imagery from the whelping region captured on the same day as the airborne photographic survey was conducted. From this satellite imagery we have extracted a variable which acts as a proxy for the ice thickness. This density variable is displayed in [Figure 2](#). Comparing the satellite data to the seal pup counts in [Figure 1](#), we see that the seal pup counts appear to be higher in the areas with high ice density, than in areas with lower ice density.

3. METHODS

This section starts with a brief introduction to point processes, and the key components of INLA and the SPDE approach which makes our proposed method computational feasible. We then describe the details of our modeling approach, three references methods, and the verification scheme used to validate and compare the methods.

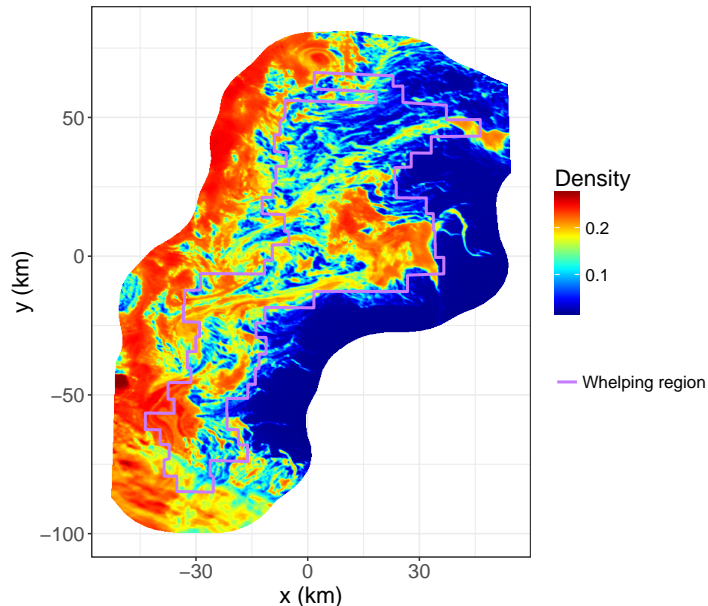


FIGURE 2. Satellite data showing ice density used as a covariate in the model fitting process.

3.1. Background.

3.1.1. *Point processes.* A spatial stochastic point process is a mathematical description of the random process through which points or locations are distributed in space. The collection of such observations is called a point pattern. In informal mathematical terms, which typically are sufficient for practical purposes, a spatial point process Y is here a random collection of points in a bounded observation region $\Omega \subset \mathbb{R}^2$ where both the number of points and their locations are random. The most fundamental type of point process is the *Poisson point process*. It may be specified by an intensity function $\lambda : \Omega \mapsto [0, \infty)$ which determines the density of points in any location in Ω . The number of points, $N(B)$, of any Borel set $B \subseteq \Omega$ is Poisson distributed with mean $\mu(B) = \int_B \lambda(\mathbf{s}) d\mathbf{s}$, i.e. $N(B) \sim \text{Pois}(\mu(B))$, and independent of $N(B^*)$ for any other non-overlapping Borel set $B^* \subseteq \Omega$.

The *Cox process* (also known as the doubly stochastic Poisson point process) introduced by Cox (1955) is a generalization of the Poisson point process where the intensity function λ is in itself stochastic. A popular special case of this hierarchical model is the *log-Gaussian Cox process* (LGCP) (Møller et al., 1998), where the intensity is assumed to be log-Gaussian; i.e. there is an underlying latent Gaussian random field Z , and given $\lambda = \exp(Z)$, Y is a Poisson point process with intensity λ . This type of model is quite flexible and useful for modeling a great variety of natural processes, in particular when only a single realization of the process is available (e.g. Diggle, 2013; Illian et al., 2008; Møller & Waagepetersen, 2003).

3.1.2. *Integrated nested Laplace approximation.* The integrated nested Laplace approximation (INLA) methodology proposed by Rue et al. (2009), and implemented in the R-package INLA (www.r-inla.org), allows for computationally feasible approximate Bayesian inference for latent Gaussian models. In latent Gaussian models, n univariate observations $\mathbf{y} = (y_1, \dots, y_n)^\top$ are assumed to be conditionally independent given m latent Gaussian variables $\mathbf{z} = (z_1, \dots, z_m)^\top$ and a set of hyperparameters $\boldsymbol{\theta}$. More precisely, the INLA implementation covers models of

the form

$$(1) \quad \begin{aligned} p(\mathbf{y}|\mathbf{z}, \boldsymbol{\theta}) &= \prod_{i=1}^n p(y_i|\eta_i, \boldsymbol{\theta}), \text{ with } \eta_i = \sum_{j=1}^m c_{ij}z_j \text{ for fixed } c_{ij}, \\ p(\mathbf{z}|\boldsymbol{\theta}) &\sim N(\boldsymbol{\mu}(\boldsymbol{\theta}), Q(\boldsymbol{\theta})^{-1}), \\ \boldsymbol{\theta} &\sim p(\boldsymbol{\theta}), \end{aligned}$$

where the latent variables \mathbf{z} may depend on additional (fixed) covariates, for a large class of models for \mathbf{y} .

For computationally fast inference it is essential that the precision matrix $Q(\boldsymbol{\theta})$ is sparse and that the parameter vector $\boldsymbol{\theta}$ is of a fairly low dimension. This covers models where the latent field is a *Gaussian Markov random field* (GMRF). For the inference, INLA utilizes several nested Laplace approximations. That is, the posterior distribution of $\boldsymbol{\theta}$ is approximated by

$$(2) \quad p(\boldsymbol{\theta}|\mathbf{y}) \approx \tilde{p}(\boldsymbol{\theta}|\mathbf{y}) \propto \frac{p(\mathbf{y}, \mathbf{z}, \boldsymbol{\theta})}{p_G(\mathbf{z}|\mathbf{y}, \boldsymbol{\theta})} \Big|_{\mathbf{z}=\mathbf{z}^*(\boldsymbol{\theta})},$$

where $p_G(\mathbf{z}|\mathbf{y}, \boldsymbol{\theta})$ is a Gaussian approximation to the full conditional distribution of \mathbf{z} , and $\mathbf{z}^*(\boldsymbol{\theta})$ is the mode of $p(\mathbf{z}|\mathbf{y}, \boldsymbol{\theta})$ for a given $\boldsymbol{\theta}$. The marginals of this low-dimensional posterior distribution are typically computed by direct numerical integration. The marginals for the latent field, $p(z_j|\mathbf{y})$, are typically computed by first obtaining a Laplace approximation $\tilde{p}(z_j|\boldsymbol{\theta}, \mathbf{y})$ similar to (2), or a Taylor approximation of that distribution, and then solve $\int \tilde{p}(z_j|\boldsymbol{\theta}, \mathbf{y}) \tilde{p}(\boldsymbol{\theta}|\mathbf{y}) d\boldsymbol{\theta}$ by numerical integration. See [Rue et al. \(2009\)](#) and [Martins et al. \(2013\)](#) for further details.

The spatial partial differential equation (SPDE) approach of [Lindgren et al. \(2011\)](#) has made it possible to perform inference with INLA also for a class of *continuous* latent fields. This is achieved by (approximately) transforming the continuous latent field to a certain GMRF, formulated through the solution of a SPDE. The key point is to approximate the continuous field $Z_0(\mathbf{s})$ by a field $Z(\mathbf{s})$ living on a triangular mesh. For a triangular mesh with m triangle vertices, we write

$$(3) \quad Z(\mathbf{s}) = \sum_{j=1}^m z_j \phi_j(\mathbf{s}),$$

where $\mathbf{z} = (z_1, \dots, z_m)^\top$ is a multivariate Gaussian random vector and $\{\phi_j(\mathbf{s})\}_{j=1}^m$ is a set of deterministic linearly independent basis functions which are piecewise linear between the vertices and chosen such that $\phi_j(\mathbf{s})$ is 1 at vertex j , and 0 at all other vertices. A consequence of the representation in (3) is that $Z(\mathbf{s})$ is fully determined by \mathbf{z} : $Z(\mathbf{s})$ takes the value z_j at vertex j while its values inside the triangles are determined by linear interpolation.

Let us further equip $Z_0(\mathbf{s})$ with the Matérn covariance function

$$(4) \quad \text{Cov}(Z_0(\mathbf{s}), Z_0(\mathbf{t})) = \frac{\sigma^2}{2^{\nu-1}\Gamma(\nu)} (\kappa\|\mathbf{t} - \mathbf{s}\|)^\nu K_\nu(\kappa\|\mathbf{t} - \mathbf{s}\|),$$

where $\nu > 0$ is a smoothing parameter, K_ν is the modified Bessel function of the second kind, $\kappa > 0$ is a scaling parameter and σ^2 is the marginal variance. Lending on this type of latent field being a solution to a certain SPDE, the precision matrix Q of \mathbf{z} takes an analytical form which can be approximated by a sparse matrix \tilde{Q} . Since $Z(\mathbf{s})$ is completely determined by \mathbf{z} , this allows continuous field computations to be carried out approximately using the INLA implementation. Note that following certain guidelines for constructing the triangular mesh, the approximation error is typically small ([Lindgren et al., 2011](#); [Simpson et al., 2012](#)).

For a complete introduction and review of the INLA framework, including the SPDE approach, see [Blangiardo & Cameletti \(2015\)](#) and [Rue et al. \(2016\)](#).

3.2. Estimating seal pup production with SPDE-INLA. We assume the seal pup production in the whelping ground A follows a log-Gaussian Cox process (LGCP). However, the exact positions of the counted seal pups are not available. Instead, the seal pup counts are provided as aggregated counts per photo. Thus, our data are point process data aggregated

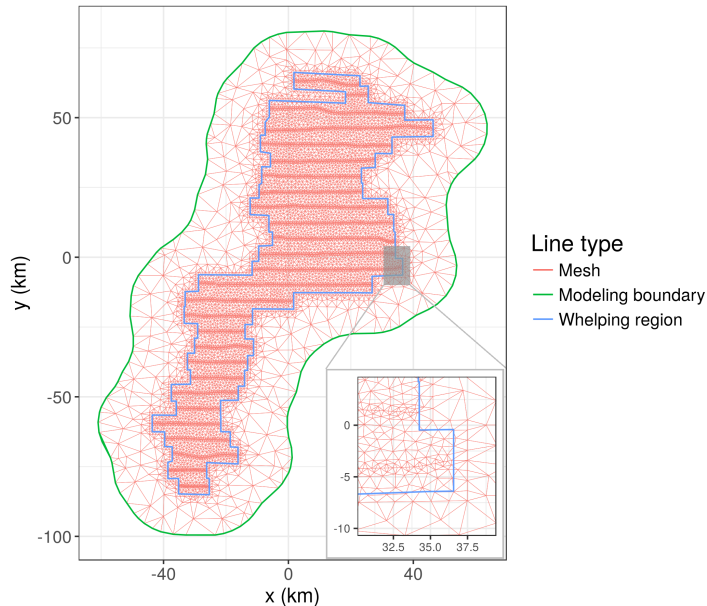


FIGURE 3. The triangular mesh used in the SPDE-INLA analysis. The bottom right corner shows a zoomed in version of the mesh for the grey area above.

to counts on an irregular lattice, as opposed to the actual point patterns. This excludes the use of the approach proposed by [Simpson et al. \(2016\)](#) who fit LGCPs using the SPDE-INLA framework by directly approximating the likelihood function of the LGCP. Rather, we expand the framework of [Rue et al. \(2009, Section 5.5\)](#) who suggest using INLA to approximate the LGCP by fitting a Poisson spatial regression model to aggregated counts on a regular lattice. As the photos do not compose a regular lattice, we use the SPDE framework to extend this to irregular lattices.

The continuous domain latent field we use in the modeling takes the form

$$(5) \quad Z_0(\mathbf{s}) = \alpha + \boldsymbol{\beta}^\top \mathbf{x}(\mathbf{s}) + f(\mathbf{s}),$$

where α is an intercept term, $\boldsymbol{\beta}$ are regression coefficients for $\mathbf{x}(\mathbf{s}) = (q(\mathbf{s}), s_1, s_2, s_1 s_2)^\top$, with $q(\mathbf{s})$ containing the density variable from the satellite imagery, while the remaining components model linear spatial effects. Finally, $f(\mathbf{s})$ is a continuous Gaussian random field with the Matérn covariance function given in (4) to model non-linear spatial dependence not captured by the covariates in \mathbf{x} . In order to make the intercept term identifiable, we restrict $f(\mathbf{s})$ to integrate to zero over the modeling region. Due to poor identifiability, we fix the Matérn smoothing parameter at $\nu = 2$, as is common when applying the INLA framework. The other hyperparameters related to the latent field are equipped with default priors specified by the INLA software. For our mesh these are $\theta_1 \sim N(1.328, 10)$ and $\theta_2 \sim N(-2.594, 10)$, where $\theta_1 = \log(\tau)$ and $\theta_2 = \log(\kappa)$, and $\sigma^2 = 1/(4\pi\kappa^2\tau^2)$. The intercept term α is assigned the improper prior $N(0, \infty)$ while $\boldsymbol{\beta} \sim N(0, 1000\mathcal{I}_4)$, where \mathcal{I}_4 denotes the 4×4 dimensional identity matrix. As all these priors are vague and they seem to influence the final results to a very limited degree. The alternative use of penalized complexity (PC) priors ([Simpson et al., 2017](#)) resulted in very similar final results.

The triangular mesh employed in the SPDE-INLA analysis is displayed in Figure 3. Note that the mesh has a finer resolution around the photos and a coarser resolution elsewhere, where fine resolution detail of the latent field cannot be easily estimated. To overcome boundary effects, we extend the area that is modeled quite a bit beyond the whelping region ([Lindgren et al., 2011](#)).

The aim of the analysis is to estimate the total number of seal pups, $N(\Omega)$, in the whelping region Ω , indicated in blue in Figure 3. Let $N(A_i)$ for $i = 1, \dots, n$ denote the number of seal pups in each of the $n = 2792$ photos with domains $A_i \subset \Omega$ for $i = 1, \dots, n$. As per the LGCP

formulation, conditional on the latent field Z , $N(A_i)$ is Poisson distributed with parameter $\lambda = \int_{A_i} \exp(Z(\mathbf{s})) \, d\mathbf{s}$, i.e.

$$(6) \quad N(A_i) | Z \sim \text{Pois}\left(\lambda = \int_{A_i} \exp(Z(\mathbf{s})) \, d\mathbf{s}\right), \quad i = 1, \dots, n.$$

We thus fit our data with the INLA software using the model formulation in (1) with the Poisson data likelihood (6), an underlying continuous random field as given in (5), the associated discrete field given in (3) and the aforementioned prior distributions.

The posterior predictive distribution for $N(\Omega)$ is given by

$$(7) \quad \begin{aligned} p(N(\Omega) | N(A_1), \dots, N(A_n)) &= \int p(N(\Omega), Z | N(A_1), \dots, N(A_n)) \, dZ \\ &= \int p(N(\Omega) | Z) p(Z | N(A_1), \dots, N(A_n)) \, dZ. \end{aligned}$$

The INLA software produces posterior distributions for all individual hyperparameters, and enables sampling from the posterior of the complete latent field $p(Z | N(A_1), \dots, N(A_n))$. This allows us to use a Monte Carlo approximation for the integral in (7),

$$\int p(N(\Omega) | Z) p(Z | N(A_1), \dots, N(A_n)) \, dZ \approx \frac{1}{K} \sum_{k=1}^K p(N(\Omega) | \tilde{Z}_k),$$

where \tilde{Z}_k is the k -th sample of the posterior latent field, $p(Z | N(A_1), \dots, N(A_n))$. Further, by the point process definition, $p(N(\Omega) | Z = \tilde{Z}_k) \sim \text{Pois}(\lambda = \int_{\Omega} \tilde{Z}_k(\mathbf{s}) \, d\mathbf{s})$. The integral here can be solved by e.g. a simple Riemann midpoint rule by dividing Ω into J rectangles B_1, \dots, B_J centered in $\mathbf{s}_1, \dots, \mathbf{s}_J$, and using $\int_{\Omega} \tilde{Z}_k(\mathbf{s}) \, d\mathbf{s} \approx \sum_{j=1}^J \tilde{Z}_k(\mathbf{s}_j) |B_j|$. The final approximation to the posterior predictive distribution is

$$(8) \quad p(N(\Omega) | N(A_1), \dots, N(A_n)) \approx \frac{1}{K} \sum_{k=1}^K \text{Pois}\left(\lambda = \sum_{j=1}^J \tilde{Z}_k(\mathbf{s}_j) |B_j|\right),$$

i.e. a Poisson mixture distribution.

3.3. Reference approaches. This subsection gives a brief outline of existing methodology for estimating the seal pup production.

3.3.1. Kingsley's method and the homogeneous Poisson model. The traditional approach to estimate seal pup production based on aerial photographic transect surveys is the so-called Kingsley's method (Kingsley et al., 1985). This method is fundamentally simple: For each transect T_1, \dots, T_{27} covering the space $A_{T_k} = \bigcup_{\{A_i \subset T_k\}} A_i$, compute the seal pup count $N_{T_k} = \sum_{A_i \in T_k} N(A_i)$. Then, the estimate of the total number of seal pups is

$$(9) \quad \hat{\mu}_{\text{Kingsley}}(N(\Omega)) = \frac{|A_{\Omega}|}{\sum_{k=1}^{27} |A_{T_k}|} \sum_{k=1}^{27} N_{T_k}.$$

Kingsley et al. (1985) also provide an estimate of the variance related to the abundance estimate, based on serial differences between the transects, which Salberg et al. (2008) provide a modification to. Since this method only provides a point and a variance estimate, it is difficult to properly compare it against the remaining Bayesian procedures. We will therefore not perform validation tests, as described in Section 3.4, for this method.

Kingsley's method is built on the principle of homogeneity within the whelping region. As such, a Poisson likelihood model with a homogeneous intensity λ_0 is therefore fundamentally quite similar to this approach. Using the photo area $|A_i|$ as offset, one then models $N(A_i) \sim \text{Pois}(\lambda = |A_i| \lambda_0)$, which can be fitted with standard software for generalized linear models. Under this model, the posterior predictive distribution for the total number of seal pups in the whelping region becomes

$$(10) \quad p_{\text{Hom.Pois}}(N(\Omega) | N(A_1), \dots, N(A_n)) = \text{Pois}(\lambda = |\Omega| \hat{\lambda}_0),$$

where $\widehat{\lambda}_0$ is the Maximum Likelihood (ML) estimate of λ_0 based on the photos. The formula in (10) does not account for the uncertainty involved in estimating λ_0 . To account for this, we rely on the asymptotic distribution of the ML estimator,

$$(11) \quad N(\lambda_0, \text{Var}(\widehat{\lambda}_0)),$$

where $\text{Var}(\widehat{\lambda}_0)$ is the asymptotic variance of $\widehat{\lambda}_0$, generally available as a closed form expression. Similar in spirit to (8), this yields

$$(12) \quad p_{\text{Hom.Pois}}(N(\Omega) | N(A_1), \dots, N(A_n)) \approx \frac{1}{K} \sum_{k=1}^K \text{Pois}(\lambda = |\Omega| \tilde{\lambda}_k),$$

where $\tilde{\lambda}_k$ is k -th sample from (11). In the validation tests below, we will use the predictive distribution in (12) in place of Kingsley's method.

3.3.2. Generalized additive models. The above assumption of a homogeneous seal pup intensity in the whelping region is typically not valid. Salberg et al. (2009) overcome this weakness by modeling the seal pup production by a generalized additive model based on a negative binomial likelihood. Denote by $\text{NegBin}(\mu, \kappa)$ the parametrization of the negative binomial distribution with mean μ and shape κ . The model here takes the form

$$(13) \quad N(A_j) \sim \text{NegBin}(\mu = |A_j| \exp(S(\mathbf{s}_j)), \kappa),$$

where $|A_j|$ as before is the fixed offset and $S(\cdot)$ is a spatial smoothing component given by a thin-plate smoothing regression spline (Wood, 2003). This fits overlapping cubic regressions on a set of artificial knots in space, producing a smooth, nonlinear spatial effect. A generalized cross validation (GCV) criterion is used to select the right amount of smoothing, see Salberg et al. (2009) and Øigård et al. (2010) for details about the model. For a fair comparison with our approach, we extend the approach with a covariate effect β for the satellite image density variable $q(\mathbf{s})$. That is, we extend (13) to

$$N(A_j) \sim \text{NegBin}(\mu = |A_j| \exp(S(\mathbf{s}_j) + \beta q(\mathbf{s}_j)), \kappa).$$

A wide range of software is available for fitting such GAMs. Here, we use the `gam` function in the R-package `mgcv` (Wood, 2017).

In contrast to the Poisson distribution, the negative binomial distribution is not closed under addition for different mean values. Thus, to arrive at a full posterior predictive distribution for the total seal pup count $N(\Omega)$, we need to rely on an underlying conditional independence condition stating that conditional on $S(\cdot), \beta$ and κ , the counts $N(A_j)$ and $N(A_k)$ are independent for $k \neq j$. Using this property, the posterior predictive distribution for $N(\Omega)$ can be written

$$(14) \quad p_{\text{GAM}}(N(\Omega) | N(A_1), \dots, N(A_n)) = \frac{1}{J} \sum_{j=1}^J \text{NegBin}(\mu = |B_j| \exp(\widehat{S}(\mathbf{s}_j) + \widehat{\beta} q(\mathbf{s}_j)), \widehat{\kappa}),$$

where B_j for $j = 1, \dots, J$ is a grid of Ω of size similar to the photos, centered in \mathbf{s}_j for $j = 1, \dots, J$. To account for the uncertainty in estimating $\widehat{S}(\cdot)$ and $\widehat{\kappa}$, we use the estimators' asymptotic normal distribution, as in (11) and (12) for the homogeneous Poisson model, to arrive at

$$(15) \quad p_{\text{GAM}}(N(\Omega) | N(A_1), \dots, N(A_n)) \approx \frac{1}{JK} \sum_{k=1}^K \sum_{j=1}^J \text{NegBin}(\mu = |B_j| \exp(\tilde{S}_k(\mathbf{s}_j) + \tilde{\beta}_k q(\mathbf{s}_j)), \tilde{\kappa}_k),$$

where $\tilde{S}(\cdot)_k, \tilde{\beta}_k$ and $\tilde{\kappa}_k$ are k -th samples of respectively the smooth spatial effect, the covariate effect, and the scaling parameter.

Salberg et al. (2009) rely on the negative binomial distribution instead of the Poisson distribution for the GAM by arguing that the latter is inappropriate due to overdispersion. However, the inhomogeneous intensity and the Poisson mixture in the posterior predictive distribution

may improve the fit of the Poisson model. We thus add a GAM with a Poisson distribution to our list of models to compare. That is, we also fit the model

$$(16) \quad N(A_j) \sim \text{Poisson}(\lambda = |A_j| \exp(S(\mathbf{s}_j) + \beta q(\mathbf{s}_j)))$$

using the GAM approach described above. The basic model here is thus the same as for the SPDE-INLA approach while the modeling of the spatially structured random effect and the parameter estimations are performed differently.

3.4. Verification. We compare the various modeling approaches using a cross-validation scheme where we rely on two procedures for subsetting the data. The first procedure is a standard 10-fold cross-validation setup, where we randomly remove 10% of the photos each time, such that each photo is removed exactly once. In the second procedure we remove all photos in one full transect at a time, such that each transect is removed exactly once, leaving us with 27 different subsets. For both procedures, we fit the competing models for every subset and compute posterior predictive distributions for every photo that is removed along with posterior predictive distributions for the sum of the removed photos (corresponding to the full transect for the latter procedure).

We compare the predictive performance of the various modeling approaches using two performance measures: The logarithmic score (Good, 1952) and the continuous ranked probability score (CRPS) (Matheson & Winkler, 1976), which both are proper scoring rules. Denoting a generic posterior predictive distribution by $g(x)$, the cumulative distribution function by $G(x)$, and the observed count by y_{true} , the two performance measures takes the form

$$(17) \quad \begin{aligned} \log\text{Score}(g, y_{\text{true}}) &= -\log(g(y_{\text{true}})), \\ \text{CRPS}(G, y_{\text{true}}) &= \int_{-\infty}^{\infty} (G(x) - \mathbb{1}_{\{x > y_{\text{true}}\}}(x))^2 dx, \end{aligned}$$

where $\mathbb{1}_{\{ \cdot \}}(x)$ denotes the indicator function. For both measures, smaller values reflect a better model. While the former rewards pointiness of the posterior predictive distribution by solely considering the point mass at y_{true} , the latter considers the full distribution and assesses both calibration and sharpness of the predictive distribution. Here, calibration refers to the statistical consistency between the prediction and the observation in that an event predicted with probability p should be realized with the same frequency in the observed data. Subject to calibration, a sharp predictive distribution is preferred (Gneiting & Raftery, 2007; Thorarinsdottir & Schuhen, 2018).

We further assess the calibration, or the prediction uncertainty, of the methods by looking at the coverage of the posterior predictive distributions. That is, we check how often y_{true} lies within different credibility intervals, compared to their intended coverage – small uncertainty is of no value if it is not reflecting the true uncertainty of the model. In order to mimic quantification of the prediction uncertainty for the complete whelping region as closely as possible, we perform this exercise on the transect level.

4. RESULTS

Here, we present the results obtained when applying the various models described above to per-photo count data from the 2012 survey of the Greenland sea whelping region. We model hooded and harp seals separately as their occurrences are expected to be independent conditional on the covariate information. Specifically, we compare the SPDE-INLA point process approach with the GAM-based procedure, both with a negative-binomial distribution for the counts and with the simpler Poisson distribution. As a baseline model we use a homogeneous Poisson model with no covariates, spatial term, or other random effects.

4.1. Hooded seals. Within the flight transect sparsely covering the whelping region, a total of 777 hooded seal pups were counted. The blue dots in Figure 1 show how these are spread on the 2792 photos, with between 0 and 12 pups per photo.

Figure 4 shows the mean and standard deviation of the latent field fitted using the SPDE-INLA point process procedure outlined in Section 3.2. As seen, the latent field captures the

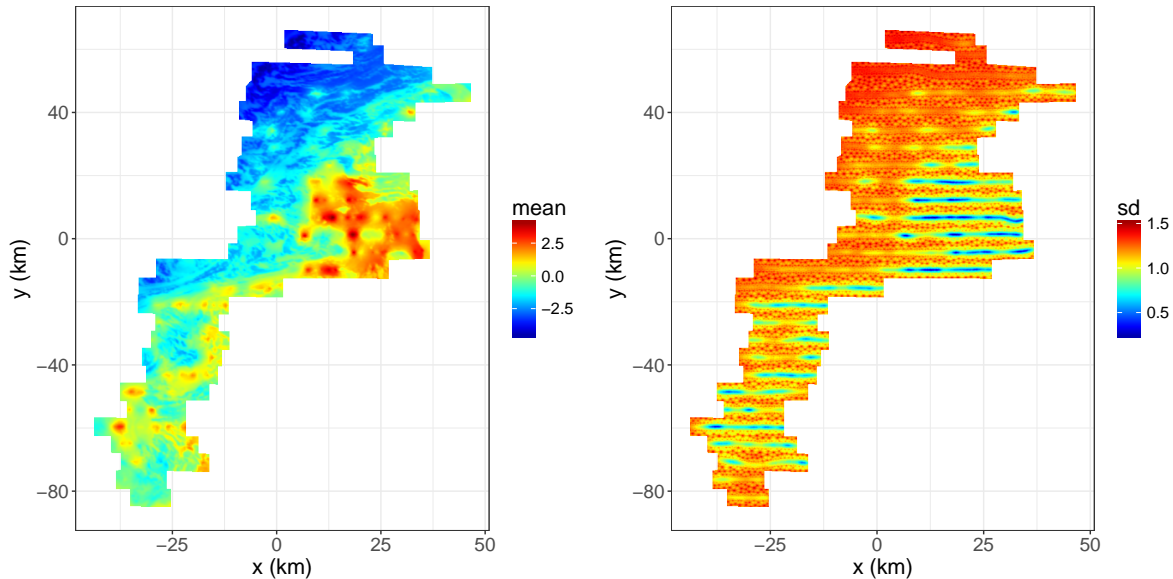


FIGURE 4. The mean and standard deviation of the latent field fitted for hooded seals with our SPDE-INLA based point process approach.

TABLE 1. Summary table for the posterior predictive distributions of the total count of hooded seal pups in the whelping region.

	mean	median	mode	IQR	0.025-quantile	0.975-quantile
Point Proc	11649	11503	11472	1699	9472	14741
GAM	11178	11157	11093	807	10075	12395
GAM Pois	11296	11292	11093	572	10467	12147
Hom Pois	11391	11384	11377	572	10586	12238

high intensity of hooded seal pups in the middle-eastern part of the whelping region. This area has a medium range ice thickness, cf. Figure 2. There is also an increased seal pup intensity further south, in particular closer to the open water. In the north, the intensity is rather low. Note however, as seen in the standard deviation plot, that the uncertainty is rather large where the intensity is low, while it is smaller where the intensity is high. This means that one is fairly certain that there are *some* seal pups in areas where seal pups are observed nearby, while there could very well exist seal pups in locations where none are observed at the neighboring observation sites.

The range of the latent field, defined as the distance at which the spatial correlation is approximately 0.1, has a posterior mean of 3.63 km, or about 2/3 of the distance between two transects. This means that in an area lying between two transects, the latent field is essentially determined by the two neighboring transects. Further, the fitted model gives the following posterior means for the intercept (α) and the fixed effects (β): $\text{mean}_\alpha = -1.37$, $\text{mean}_{\beta,q} = 9.07$, $\text{mean}_{\beta,s_1,s_2,s_{12}} = (0.07, -0.02, 3.63)$.

Figure 5 shows the posterior predictive distribution for the total pup count in the whelping region using our procedure, along with the corresponding results for the two GAM-based procedures and the homogeneous Poisson model. A simple summary of Kingsley’s method is also given for reference. Table 1 summarizes the predictive distributions. While most of the mass coincides for the four different approaches, the GAM with a negative binomial distribution yields the lowest estimates and our method the highest estimates. The homogeneous Poisson approach and the GAM with a Poisson distribution have the lowest prediction uncertainty. Here, our method has an interquartile range approximately three times larger than that of the other two methods despite all three being based on the Poisson distribution.

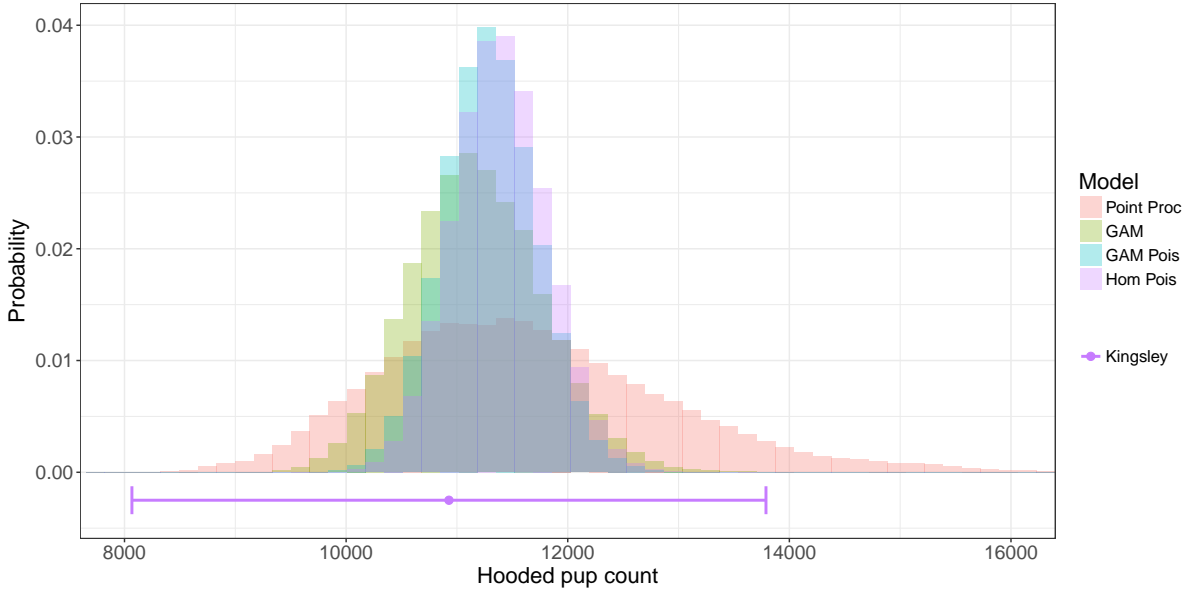


FIGURE 5. The posterior predictive distributions for the total hooded pup counts in the whelping region for the five competing models. For Kingsley’s method, we show the point estimate ± 2 times the estimated standard deviation, corresponding to an approximate 95% confidence interval under a normal distribution assumption.

TABLE 2. Validation results on photo level (one prediction per photo) and transect level (one prediction per transect), respectively. Lower and upper bounds of 90% bootstrapped confidence intervals for the scores are shown in parenthesis. Cells shown in italics are the best (smallest) per column. Those which are significantly smaller than the others (defined as having non-overlapping confidence intervals) are also bolded.

HOODED SEALS: PHOTO LEVEL

	Random 10-fold CV		Leave-out full transect	
	CRPS	logScore	CRPS	logScore
Point Proc	<i>0.18 (0.16, 0.19)</i>	<i>0.47 (0.44, 0.49)</i>	<i>0.22 (0.20, 0.25)</i>	0.54 (0.51, 0.57)
GAM	0.21 (0.19, 0.23)	0.51 (0.47, 0.53)	<i>0.22 (0.20, 0.24)</i>	<i>0.53 (0.50, 0.56)</i>
GAM Pois	0.22 (0.20, 0.24)	0.54 (0.51, 0.58)	0.24 (0.22, 0.26)	0.58 (0.54, 0.62)
Hom Pois	0.26 (0.24, 0.28)	0.69 (0.65, 0.73)	0.26 (0.24, 0.29)	0.70 (0.66, 0.74)

HOODED SEALS: AGGREGATE/TRANSECT LEVEL

	Random 10-fold CV		Leave-out full transect	
	CRPS	logScore	CRPS	logScore
Point Proc	5.43 (4.04, 6.99)	3.68 (3.51, 3.86)	9.91 (5.99, 14.80)	<i>3.67 (3.26, 4.09)</i>
GAM	5.93 (4.95, 7.00)	3.79 (3.68, 3.91)	<i>9.37 (5.66, 13.63)</i>	3.68 (3.11, 4.27)
GAM Pois	5.90 (4.49, 7.42)	3.72 (3.50, 3.96)	10.14 (5.86, 15.09)	4.14 (3.32, 5.01)
Hom Pois	<i>4.83 (3.27, 6.66)</i>	<i>3.59 (3.30, 3.90)</i>	15.57 (11.77, 19.68)	6.71 (5.91, 7.52)

Table 2 shows the results from the validation scheme applied to the four methods we compare here, as outlined in Section 3.4. At the photo level, we issue a prediction for the pup count per photo, for either 10% of the photos or all photos in a single transect at a time. Here, our method yields very good results, in particular for the random 10-fold cross-validation where observations are generally available in the neighborhood of the prediction locations. It is significantly the best

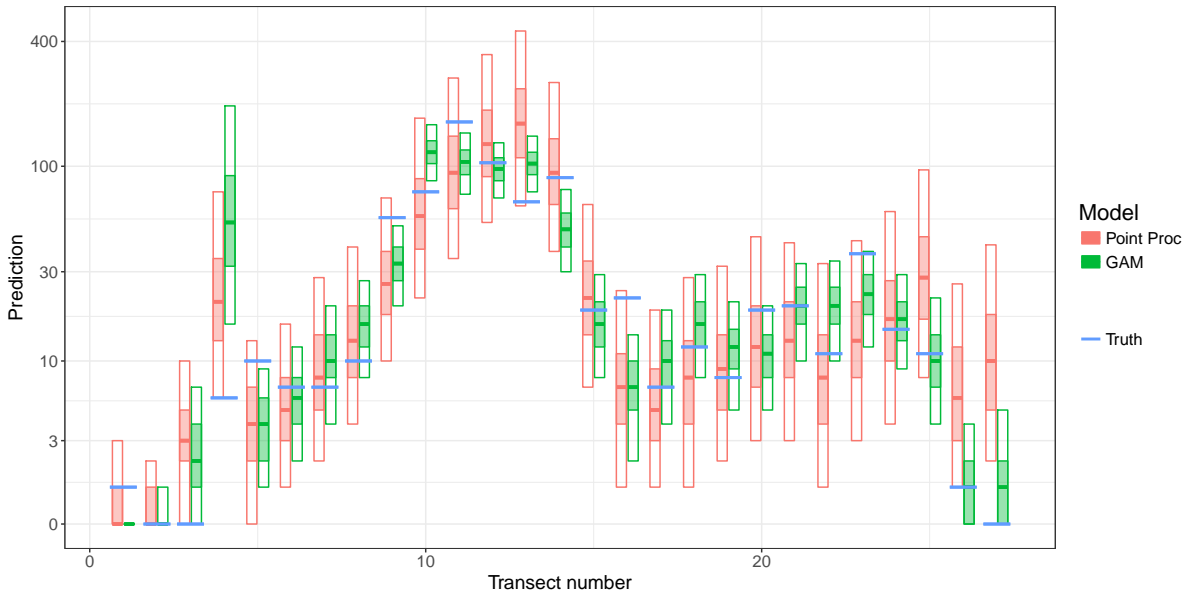


FIGURE 6. The posterior predictive distributions per transect for the SPDE-INLA point process and negative binomial GAM methods plotted against the true count for hooded seals. For each method, the solid line shows the median, the light colored box shows the 50% CI, while the transparent box shows the 90% CI. The y-axis has a $\log_{10}(x+2)$ -scale to better show differences.

method for this setting under the CRPS, defined as having non-overlapping 90% CI strictly below all others, and almost significant in terms of the logScore. When leaving out a full transect at a time, our method and the GAM version with the underlying negative binomial distribution perform very similar, and somewhat better than the others.

At the aggregate/transect level we issue a joint prediction for the total pup count per 10% of the photos or per transect, respectively. Here, the baseline homogeneous Poisson model performs very well with the random leave-out scheme, indicating that the data may be close to homogeneous across the photos. However, this does not transfer to the second set-up where we leave out one transect at a time in which case our method and the GAM with negative binomial response again perform well. As seen in Figure 1, the data do not appear homogeneous across the transects. Note that these reported scores are averages over relatively few predictions, only 10 distinct predictions for the random 10-fold cross-validation study and 27 distinct predictions for the other case. The score values are thus associated with a large degree of uncertainty.

Based on the results in Table 2, our method performs somewhat similar to the original GAM with a negative binomial response and these are both clearly superior to the other two alternatives; the two methods can only be distinguished in terms of CRPS on the photo level. Despite this, their resulting posterior predictive distributions are quite different. To get a further insight into this phenomenon, Figure 6 shows the posterior predictive distributions for the two methods per transect in the leave-out-transect setup, plotted against the true transect counts. As seen from the figure, the GAM method seems to have too narrow credibility intervals, while the SPDE-INLA point process approach appears more calibrated. In fact, the 90% CI covers the true count in $26/27 \approx 96\%$ of the transects for the point process approach, and only $18/27 \approx 67\%$ of the transects for the GAM approach. The 50% CI is covered in respectively $16/27 \approx 59\%$ and $11/27 \approx 41\%$ of the transects for the point process and GAM approaches.

4.2. Harp seals. A total of 6034 harp seal pups were observed on the 2792 photos from the aerial photographic survey. As illustrated by the red dots in Figure 1, there are much larger packs of harp seal pups than hooded seal pups, indicating a higher degree of inhomogeneity. Here, the pup count per photo ranges from 0 to 160.

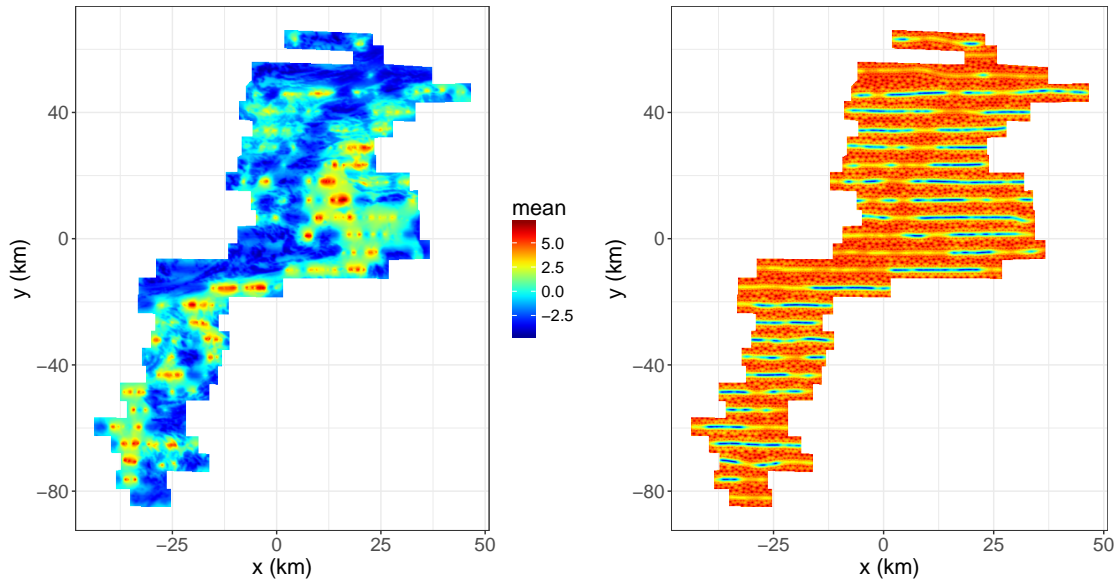


FIGURE 7. The mean and standard deviation of the latent field fitted for harp seals with our SPDE-INLA based point process approach.

TABLE 3. Summary table for the posterior predictive distributions for the total number of harp seal pups in the whelping region.

	mean	median	mode	IQR	0.025-quantile	0.975-quantile
Point Proc	147919	127965	110996	72347	69267	357185
GAM	98617	98035	91876	12895	81023	119349
GAM Pois	84852	84852	84910	1536	82681	87094
Hom Pois	88424	88419	88389	1581	86149	90742

Figure 7 shows the mean and standard deviation of the fitted latent field using our procedure. Compared to the latent field for the hooded seal pups in Figure 4, the mean field here has a much higher degree of spatial variation with higher and steeper peaks. However, the locations where the seal pups mainly appear are similar to those for the hooded seal pups, except for some additional colonies in the north and north-west of the region. Otherwise, the properties of the two fields are fairly similar. The range of the latent field has a posterior mean of 2.89, slightly smaller than for the hooded seals. The fitted model gives the following posterior means for intercept (α) and fixed effects (β): $\text{mean}_{\alpha} = -2.77$, $\text{mean}_{\beta,q} = 14.70$, $\text{mean}_{\beta,s_1,s_2,s_{12}} = (0.03, 0.01, -0.003)$. Note that the covariate effects are stronger for the harps than the hooded seals.

Figure 8 shows the posterior predictive distribution for the total number of harp seal pups in the whelping region using our procedure, along with the corresponding results for the two GAM procedures and the homogeneous Poisson model. A simple summary of Kingsley’s method is also given for reference. Table 3 summarizes these distributions. Our SPDE-INLA point process approach is extremely vague about the total harp seal pup count, essentially saying that the total number of seal pups could very well be above 250 000, but also less than 100 000. In contrast, the negative binomial GAM method’s upper tails ends at about 130 000 seal pups, while the other two Poisson methods both have upper tails below 100 000.

Table 4 shows the results from the validation procedure for the harp seals, yielding similar model rankings as for the hooded seals. On photo level, the SPDE-INLA point process approach gives a significantly better CRPS and logScore under random 10-fold cross-validation. Leaving out full transects gives no significantly best method although the Poisson GAM method tends to generally do well here. However, these average scores are associated with a very high degree of uncertainty.

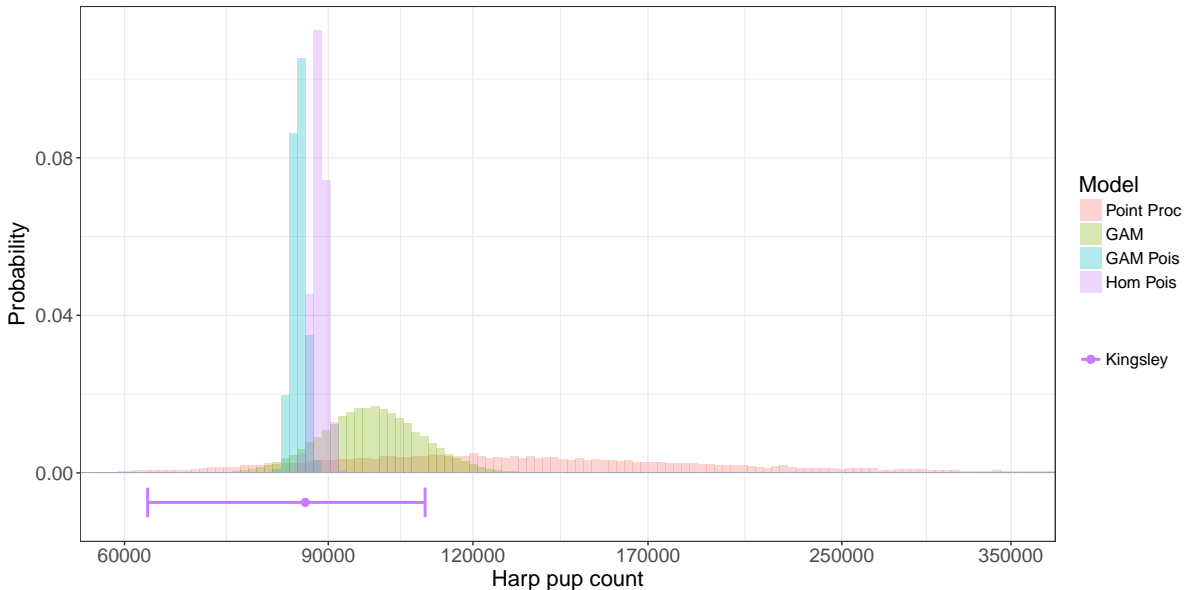


FIGURE 8. The posterior predictive distributions for the total harp pup counts in the whelping region for the five different approaches. The x-axis is plotted on log-scale. For Kingsley’s method, we show the point estimate ± 2 times the estimated standard deviation, corresponding to an approximate 95% confidence interval under a normal distribution assumption.

As for the hooded seals, we take a closer look at the SPDE-INLA point process and negative binomial GAM methods to better understand how well their different estimates of the prediction uncertainty match the actual uncertainty, see Figure 9. As expected, the GAM method has a much narrower credibility intervals which too often fail to cover the true seal pup count in the transect, while our method shows much better calibration. Out of the 27 transects, the 90% credibility intervals for the SPDE-INLA point process and the negative binomial GAM approaches covers the true count in respectively $24/27 \approx 89\%$ and $18/27 \approx 67\%$ of the transects. The corresponding coverages for the 50% interval are $14/27 \approx 52\%$ and $11/27 \approx 41\%$, respectively. Thus, it is clear that the negative binomial GAM method is underdispersive, while our procedure seems fairly well calibrated.

5. CONCLUSIONS AND DISCUSSION

We have presented a point process based approach to estimate seal pup production based on observational data from an aerial photographic survey. Using the SPDE-INLA framework, we fit a Bayesian hierarchical model with Poisson counts following a log-Gaussian Cox process model formulation. As an additional contribution to seal pup abundance estimation, we adopt the use of satellite imagery as covariates in the modeling process, to act as a proxy for ice thickness. The approach is applied to 2012 survey data from the Greenland Sea, with both harp and hooded seal pup counts, and compared to several reference methods.

The competing methods are compared in a comprehensive cross-validation study. Our proposed approach generally performs best locally, while no method stands out as the best on a more regional scale. However, this lack of discrimination in the comparison at the regional scale is not surprising given the relatively small size of our data set, see e.g. the discussion and examples in (Thorarinsdottir & Schuhen, 2018). The most distinguishing character of our method is the large prediction uncertainty compared to the other methods. Our analysis suggests that the wide uncertainty bounds are indeed necessary to issue calibrated predictions, suggesting that the amount of data collected in the aerial photographic survey might not be sufficient to obtain reliable estimates of the total seal pup production in the whelping region.

TABLE 4. Validation results on photo level (one prediction per photo) and transect level (one prediction per transect), respectively. Lower and upper bounds of 90% bootstrapped confidence intervals for the scores are shown in parenthesis. Cells shown in italics are the best (smallest) per column. Those which are significantly smaller than the others (defined as having non-overlapping confidence intervals) are also bolded.

HARP SEALS: PHOTO LEVEL				
	Random 10-fold CV		Leave-out full transect	
	CRPS	logScore	CRPS	logScore
Point Proc	<i>1.14 (1.01, 1.27)</i>	<i>0.95 (0.91, 1.00)</i>	1.96 (1.72, 2.20)	1.28 (1.22, 1.33)
GAM	1.78 (1.58, 2.00)	1.17 (1.11, 1.22)	<i>1.90 (1.67, 2.13)</i>	<i>1.27 (1.21, 1.33)</i>
GAM Pois	2.32 (2.10, 2.55)	2.09 (2.00, 2.17)	2.46 (2.22, 2.71)	2.17 (2.08, 2.26)
Hom Pois	2.68 (2.44, 2.94)	2.50 (2.45, 2.55)	2.69 (2.45, 2.95)	2.52 (2.46, 2.57)

HARP SEALS: AGGREGATE/TRANSECT LEVEL				
	Random 10-fold CV		Leave-out full transect	
	CRPS	logScore	CRPS	logScore
Point Proc	95.98 (51.20, 148.78)	6.57 (5.93, 7.33)	152.95 (111.93, 198.59)	<i>6.49 (5.98, 6.94)</i>
GAM	88.33 (70.94, 106.87)	<i>6.45 (6.31, 6.62)</i>	96.70 (61.05, 139.91)	7.00 (6.24, 7.76)
GAM Pois	<i>60.93 (42.57, 79.87)</i>	8.03 (6.83, 9.22)	<i>55.96 (39.62, 74.51)</i>	8.42 (7.34, 9.39)
Hom Pois	69.67 (45.62, 93.94)	7.69 (6.58, 8.73)	91.19 (61.09, 124.17)	7.96 (7.32, 8.57)

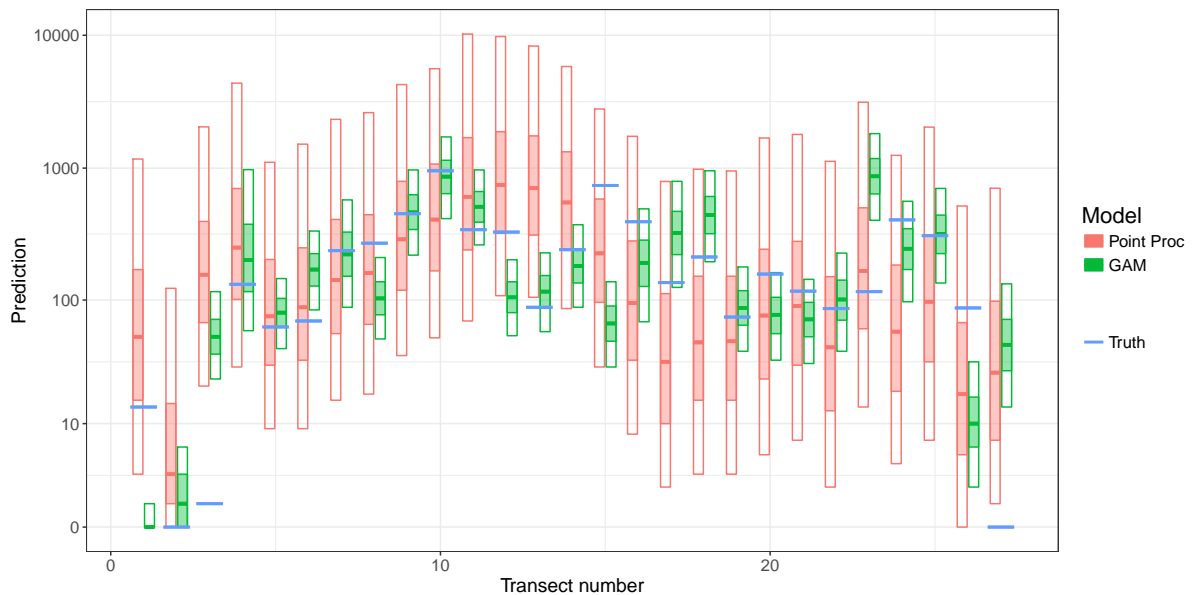


FIGURE 9. The posterior predictive distributions per transect for the SPDE-INLA point process and negative binomial GAM methods plotted against the true count for harp seal pups. For each method, the solid line shows the median, the light colored box shows the 50% CI, while the transparent box shows the 90% CI. The y-axis takes a $\log_{10}(x+2)$ -scale to better show differences.

The difference in the amount of prediction uncertainty is likely due to the fact that we build a full Bayesian model from the ground with priors on parameters, while the other methods are merely pseudo-Bayesian procedures. In particular, we do not include smoothing parameter uncertainty in the GAM approaches. While it would be possible to extend the GAM approaches

in this direction, see e.g. Wood (2016), we have here aimed to replicate the implementation of Salberg et al. (2009) for the comparison.

Salberg et al. (2009) found that a negative binomial likelihood was necessary in order to obtain a good fit to the data. However, the conclusions of our analysis indicate that a more careful and comprehensive assessment of both the model uncertainty and the spatial inhomogeneities may warrant the use of the simpler Poisson likelihood.

ACKNOWLEDGMENTS

Martin Jullum and Thordis Thorarinsdottir acknowledge the support of The Research Council of Norway through grant 240838 “Model selection and model verification for point processes”. Fabian Bachl was supported by EPSRC grant EP/K041053/1 “Modelling spatial distribution and change from wildlife survey data”. We thank Tor Arne Øigård for helpful discussions and for assisting with the photographic survey data which were provided by the Norwegian Institute of Marine Research, Øivind Due Trier for retrieving the satellite image data and Dawid Lawrence Miller for helpful discussions regarding the various inference approaches.

REFERENCES

- [1] BLANGIARDO, M. & CAMELETTI, M. (2015). *Spatial and Spatio-temporal Bayesian Models with R - INLA*. Wiley.
- [2] COX, D. R. (1955). Some statistical methods connected with series of events. *Journal of the Royal Statistical Society. Series B (Methodological)* , 129–164.
- [3] DIGGLE, P. J. (2013). *Statistical analysis of spatial and spatio-temporal point patterns*. Chapman and Hall/CRC.
- [4] GNEITING, T. & RAFTERY, A. E. (2007). Strictly proper scoring rules, prediction, and estimation. *Journal of the American Statistical Association* **102**, 359–378.
- [5] GOOD, I. J. (1952). Rational decisions. *Journal of the Royal Statistical Society. Series B (Methodological)* , 107–114.
- [6] HASTIE, T. & TIBSHIRANI, R. (1990). *Generalized additive models*. Wiley Online Library.
- [7] ICES (2014). Report of the ICES/NAFO working group on harp and hooded seals (WGHARP). Tech. rep., ICES CM 2014/ACOM:20, Quebec City, Quebec, Canada.
- [8] ILLIAN, J., PENTTINEN, A., STOYAN, H. & STOYAN, D. (2008). *Statistical analysis and modelling of spatial point patterns*, vol. 70. John Wiley & Sons.
- [9] KINGSLEY, M., STIRLING, I. & CALVERT, W. (1985). The distribution and abundance of seals in the Canadian High Arctic, 1980–82. *Canadian Journal of Fisheries and Aquatic Sciences* **42**, 1189–1210.
- [10] KOVACS, K. M. & LAVIGNE, D. (1986). *Cystophora cristata*. *Mammalian Species* , 1–9.
- [11] LINDGREN, F., RUE, H. & LINDSTRÖM, J. (2011). An explicit link between Gaussian fields and Gaussian Markov random fields: The stochastic partial differential equation approach. *Journal of the Royal Statistical Society: Series B (Statistical Methodology)* **73**, 423–498.
- [12] MARTINS, T. G., SIMPSON, D., LINDGREN, F. & RUE, H. (2013). Bayesian computing with INLA: New features. *Computational Statistics & Data Analysis* **67**, 68–83.
- [13] MATHESON, J. E. & WINKLER, R. L. (1976). Scoring rules for continuous probability distributions. *Management science* **22**, 1087–1096.
- [14] MØLLER, J., SYVERSVEEN, A. R. & WAAGEPETERSEN, R. P. (1998). Log Gaussian Cox processes. *Scandinavian journal of statistics* **25**, 451–482.
- [15] MØLLER, J. & WAAGEPETERSEN, R. P. (2003). *Statistical inference and simulation for spatial point processes*. CRC Press.
- [16] ØIGÅRD, T. A., HAUG, T. & NILSSEN, K. T. (2014a). Current status of hooded seals in the Greenland Sea. victims of climate change and predation? *Biological conservation* **172**, 29–36.
- [17] ØIGÅRD, T. A., HAUG, T. & NILSSEN, K. T. (2014b). From pup production to quotas: current status of harp seals in the Greenland Sea. *ICES Journal of Marine Science: Journal du Conseil* **71**, 537–545.

- [18] ØIGÅRD, T. A., HAUG, T., NILSSEN, K. T. & SALBERG, A.-B. (2010). Estimation of pup production of hooded and harp seals in the Greenland Sea in 2007: Reducing uncertainty using generalized additive models. *Journal of Northwest Atlantic Fishery Science* **42**, 103–123.
- [19] RUE, H., MARTINO, S. & CHOPIN, N. (2009). Approximate Bayesian inference for latent Gaussian models using integrated nested Laplace approximations (with discussion). *Journal of the Royal Statistical Society, Series B* **71(2)**, 319–392.
- [20] RUE, H., RIEBLER, A., SØRBYE, S. H., ILLIAN, J. B., SIMPSON, D. P. & LINDGREN, F. K. (2016). Bayesian computing with INLA: A review. *arXiv preprint arXiv:1604.00860* .
- [21] SALBERG, A.-B., HAUG, T. & NILSSEN, K. T. (2008). Estimation of hooded seal (*cystophora cristata*) pup production in the Greenland Sea pack ice during the 2005 whelping season. *Polar Biology* **31**, 867.
- [22] SALBERG, A.-B., ØIGÅRD, T. A., STENSON, G. B., HAUG, T. & NILSSEN, K. T. (2009). Estimation of seal pup production from aerial surveys using generalized additive models. *Canadian Journal of Fisheries and Aquatic Sciences* **66**, 847–858.
- [23] SERGEANT, D. E. (1974). A rediscovered whelping population of hooded seals *cystophora cristata* erleben and its possible relationship to other populations. *Polarforschung* **44**, 1–7.
- [24] SERGEANT, D. E. (1991). Harp seals, man and ice. *Canadian Journal of Fisheries and Aquatic Sciences* **114**, 1–153.
- [25] SIMPSON, D., ILLIAN, J. B., LINDGREN, F., SØRBYE, S. H. & RUE, H. (2016). Going off grid: computationally efficient inference for log-Gaussian Cox processes. *Biometrika* **103**, 49–70.
- [26] SIMPSON, D., LINDGREN, F. & RUE, H. (2012). In order to make spatial statistics computationally feasible, we need to forget about the covariance function. *Environmetrics* **23**, 65–74.
- [27] SIMPSON, D., RUE, H., RIEBLER, A., MARTINS, T. G., SØRBYE, S. H. et al. (2017). Penalising model component complexity: A principled, practical approach to constructing priors. *Statistical Science* **32**, 1–28.
- [28] THORARINSDOTTIR, T. L. & SCHUHEN, N. (2018). Verification: assessment of calibration and accuracy. In *Statistical Postprocessing of Ensemble Forecasts*. Elsevier, pp. 155–186.
- [29] WOOD, S. (2017). *Generalized Additive Models: An Introduction with R*. Chapman and Hall/CRC, 2nd ed.
- [30] WOOD, S. N. (2003). Thin-plate regression splines. *Journal of the Royal Statistical Society (B)* **65**, 95–114.
- [31] WOOD, S. N. (2016). Just another Gibbs additive modeler: Interfacing JAGS and mgcv. *Journal of Statistical Software* **75**, 1–15.